Measurement of select transition strengths and autoionizing lifetimes in atomic oxygen

A. V. Smith, T. D. Raymond, and M. E. Riley

Sandia National Laboratories, Albuquerque, New Mexico 87185

We have located the $(^2D°)4p'\,^3F$ and $(^2D°)3p'\,^3P$ autoionizing states of atomic oxygen and measured the autoionization-dominated lifetimes for the $(^2D°)3p'\,^{1,3}P$, and $(^2D°)3p'\,^3D,^3F$ states. In addition, we have measured transition strengths for the $(^4S°)3p\,^3P$ to $(^2D°)3s'\,^3D°$ and $(^2D°)3s'\,^3D°$ to $(^2D°)3p'\,^{1,3}P,^3D,^3F$ transitions, and characterized the $2p^4\,^3P$ to $(^4S°)3p\,^3P$ two-photon resonance for saturating light intensities. In making these original measurements, we use a variety of multiphoton-ionization methods, including Rabi-oscillation and damped-Rabi-oscillation methods.

PACS number(s): 32.70.Cs, 32.80.Dz, 32.80.Rm

I. INTRODUCTION

The ground-state electronic configuration of atomic oxygen is $1s^2 2s^2 2p^4$. If one of the $2p$ electrons is excited, the remaining electrons can combine to form one of the three relatively low-energy core states, $^4S°$, $^2D°$, or $^2P°$. As Fig. 1 shows, each of these cores states can combine with the excited electron to form a series of states whose energies converge to the associated $^4S°$, $^2D°$, or $^2P°$ ion energy. The $^4S°$ core forms a series of triplet and quintet states, while the $^2D°$ and $^2P°$ cores form singlet and triplet states. By convention, states with the $^2D°$ core are designated with a prime and those with a $^2P°$ core are designated with a double prime. Those states lying above the lowest-energy ionization limit, that is, states with $^2D°$ and $^2P°$ cores, can autoionize due to interactions between the excited electron and the core. In this process the core relaxes to a lower-energy state and the excess energy is imparted to the ejected electron.

The present state of knowledge of oxygen spectroscopy is that the energy levels of the bound states [1] and the odd-parity autoionizing states [2] associated with the $^2D°$ and $^2P°$ cores are extensively cataloged. In addition, the lifetimes and branching ratios for many of these odd-parity autoionizing states have been measured [3]. In contrast, only a few of the even-parity autoionizing levels have been located [4,5] and only one lifetime has been reported [5]. We have located the even-parity autoionizing states $4p'\,^3F$ and $3p'\,^3P$ and measured autoionization rates for the $3p'\,^{1,3}P$ and $3p'\,^3D,^3F$ even-parity states. In addition, we have measured transition strengths for the electric-dipole-allowed transitions $3p\,^3P$ to $3s'\,^3D°$ and $3s'\,^3D°$ to $3p'\,^{1,3}P,^3D,^3F$. The former is a "core-changing" transition so this measurement along with the autoionization lifetimes might serve as benchmarks for calculations of the core-electron configurations and their interactions with the excited electron. We also characterized the $2p^4\,^3P$ to $3p\,^3P$ two-photon resonance for high-intensity light. This will find application in calibrating two-photon resonant-fluorescence and resonant-ionization measurements in oxygen.

II. APPARATUS

We use a variety of measurement techniques, all based on multiphoton ionization of atomic oxygen. In this section we describe the apparatus common to all the measurements, and in subsequent sections we will discuss the various measurement methods in detail. We usually use three tunable lasers to sequentially excite O atoms to an autoionizing level, detecting the O^+ ions in a time-of-flight mass spectrometer. An atomic-oxygen beam is derived from a microwave-driven discharge in a mixture of O_2 and He and the laser beams intersect it at 90°, so the transitions are nearly Doppler free.

Figure 2 is a block diagram of our equipment. One of the lasers provides 226-nm light to pump the $2p^4\,^3P - 3p\,^3P$ two-photon transition. A single-mode cw dye laser pumped by an Ar^+ laser generates 573-nm light that is pulse amplified in a series of dye cells pumped by the second-harmonic light from an injection-seeded,
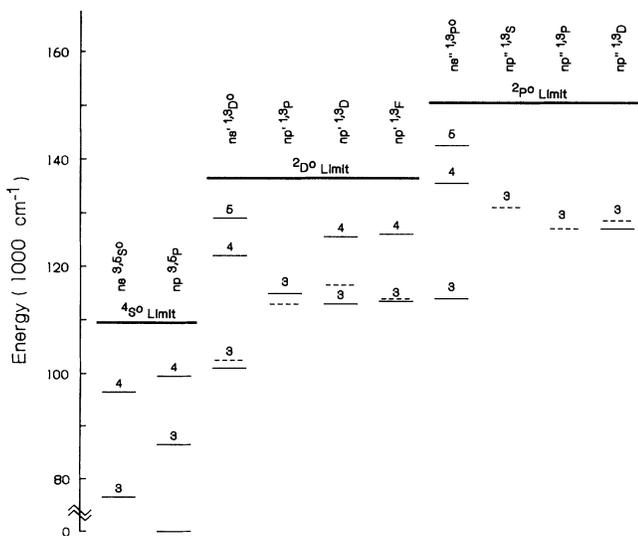
FIG. 1. Partial energy-level diagram for atomic oxygen. Solid lines represent triplet levels and dashed lines represent singlet levels.
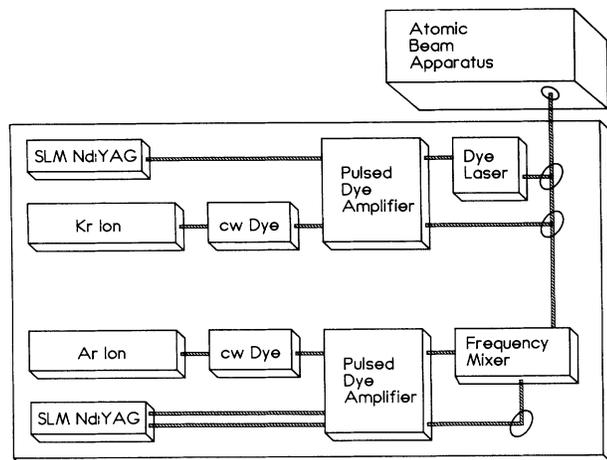
FIG. 2. Schematic diagram of the experimental apparatus (SLM means single longitudinal mode).

FIG. 3. Diagram of the atomic-beam and mass-spectrometer apparatus.

single-longitudinal-mode, Q-switched Nd:YAG laser (where YAG denotes yttruim aluminum garnet). The amplified light is frequency doubled and summed with the 1.06-μm Nd:YAG fundamental in two potassium dihydrogen phosphate (KDP) crystals to generate a few millijoules of 226-nm light. Because this light has good pulse-to-pulse stability in frequency, pulse energy, and spatial and temporal profile, it produces an excited-state oxygen $3p\ ^3P$ population that varies little from pulse to pulse.

A second single-mode cw dye laser is usually used to produce light resonant with the transition under study. It operates near 800 nm and is pumped by a Kr^+ laser. Its light is also pulse amplified in dye cells (Exciton dye LDS821) pumped by a second injection-seeded, single-longitudinal-mode Nd:YAG laser. We looked for chirps or frequency shifts of this amplified light relative to the cw light, and compared the bandwidth of the amplified light with the Fourier transform of its pulse shape, by passing it through a high-finesse confocal étalon and independently monitoring the transmission of the cw and amplified light while scanning the cw dye-laser frequency through the étalon's transmission maximum. We find that the pulsed light is shifted by less than 5 MHz from the cw light both at the center of the gain profile of the dye (800 nm) and at the blue end of the gain profile (788 nm). The measured bandwidth is consistently 10–15 MHz greater than the transform-limited width. This excess width is probably an artifact due to fluctuations in the cw-light frequency. In any case, we take account of this excess width in analyzing our measurements. The second Nd:YAG laser also pumps the third tunable dye laser, a grating-tuned laser that can be operated on a single longitudinal mode with the insertion of an intracavity étalon.

The pulse duration of each of the three lasers is nominally 4.5 ns full width at half maximum (FWHM) with a Gaussian time profile. In practice we find some variation in pulse shape and duration depending on the alignment and intensity of the 532-nm pump light at the dye amplifier chains. Consequently, to ensure the best accu-

racy in our measurements, we measure the actual temporal profile for each data set and use that in our analysis.
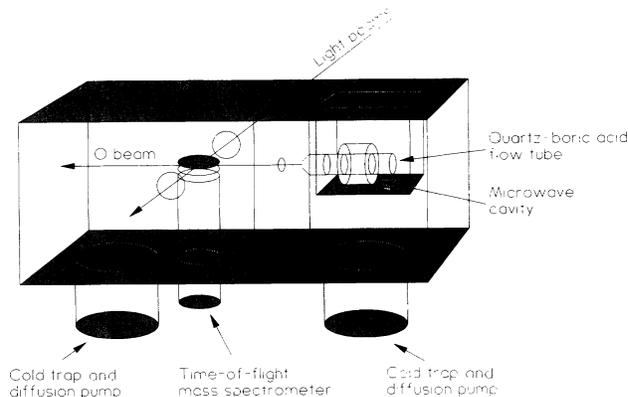
The light beams are always linearly polarized with their electric field parallel to the static electric field of the mass spectrometer. Choosing the quantization axis along the fields ensures that all optical transitions satisfy $\Delta m_J = 0$ and the static field does not mix the m_J levels.

The oxygen beam is produced in the two-chamber vacuum system diagramed in Fig. 3. In the higher-pressure chamber, a mixture of equal parts of O_2 and He flows through a microwave discharge, where the O_2 is dissociated. The discharge is contained by a quartz flow tube coated with boric acid to minimize oxygen recombination on the walls. A small orifice in the flow tube acts in conjunction with the skimmer separating the two vacuum chambers to collimate the O beam to an angle of approximately 25 mrad in the second chamber, where it passes through the sample region of the time-of-flight mass spectrometer. The mass spectrometer serves primarily to separate the O^+ ions from other ions produced by the high-intensity, 226-nm light. The accelerating electric field in its sampled region is typically 50–250 V/cm, and the 80-cm flight tube is maintained at -1 kV. The ion signal is amplified in a Johnston particle multiplier. We estimate that the atomic-oxygen density in the sampled region is 10^8 cm^{-3}, while the ambient pressure in the second chamber is approximately 3×10^{-7} Torr ($\sim 10^{10}$ cm^{-3}).

III. TWO-PHOTON RESONANT, THREE-PHOTON IONIZATION LINE SHAPES

The intent of this measurement is to compare actual two-photon resonant, three-photon ionization line shapes for the $2p^4\ ^3P$ (ground state) to $3p\ ^3P$ transition, with those calculated from theoretic values for the two-photon-absorption cross section, the upper-level photoionization cross section, and the light-induced ac Stark shifts of the two levels. The line shape depends also on the temporal and spatial profiles of the light pulse and these are considered in the comparison.

Dixit, Levin, and McKoy [6] have calculated the two-photon absorption cross section, photoionization cross section, and ac Stark shift using quantum-defect methods. Others [7] have also calculated the two-photon absorption cross sections. These calculations are consistent, spanning a range of only 20%. They also agree well with the value measured by Bamford et al. [8]. Similarly, Dixit, Levin, and McKoy's [6] calculated cross section of 4.15×10^{-19} cm^2 for photoionization of the $3p\ ^3P$ state by 226-nm light agrees with the measured value of Bamford et al. of $5.3 \pm 2.0 \times 10^{-19}$ cm^2. Thus, of the three values that contribute to the line shapes, only the ac Stark shifts have not been measured. Since our line-shape measurement is quite sensitive to that shift, it may be considered a test of the ac Stark coefficient calculated by Dixit, Levin, and McKoy [6].

We measure the line shape by frequency scanning the 226-nm light through the ground-state $(2p^4\ ^3P)$ $J=2$ to $3p\ ^3P$ $J=1$ transition while collecting O$^+$ ions. To produce a light beam with a well-characterized spatial profile, we filter it by first focusing it through a 300-μm-diam pinhole, then expanding it over a 4-m path, and finally aperturing the resulting Airy pattern at its first null. This light is then focused into the oxygen beam. A small fraction of the beam is picked off by a beam splitter after the focusing lens but before the vacuum chamber, and a glass microscope cover slip that fluoresces in the visible is placed at the focus. The fluorescent spot is imaged on the focal plane of a video camera using a microscopic-objective lens. From the video image we measure the intensity distribution at the focus for individual laser pulses. We find that the distribution is nearly Gaussian in transverse profile with a diameter of 22 ± 2 μm (FWHM), in agreement with the profile calculated from the observed Airy pattern and strength of the focusing lens. In order to minimize the effect of varying focal-spot size along the direction of propagation of the light beam, we collect ions only over a 2 mm length along the focus by placing an aperture in the ion-collection optics of the time-of-flight spectrometer. The focal point of the light is carefully centered axially to ± 1.5 mm within the 2-mm aperture. Because the light is linearly polarized, only the $m_J = \pm 1$ magnetic sublevels of $3p\ ^3P$ are populated for this particular two-photon transition [6]. The time profile of the light pulse is nearly Gaussian with a duration of approximately 4.5 ns (FWHM). We monitor the energy of each light pulse using a pyroelectric detector calibrated to $\pm 5\%$. To minimize the effects of fluctuations in energy of the light pulses, we accept data only when the pulse energy falls within a window of 10% on either side of a nominal energy.

Figure 4 shows measured line shapes for two pulse energies, along with modeled line shapes. The ion signal is increasing near the right-hand edge of the scans due to the nearby $J=2$ to $J=2,0$ transitions which are not included in the model. In modeling the line shapes, we use Dixit, Levin, and McKoy's [6] values for the two-photon cross section and photoionization cross section but vary the ac-Stark-shift coefficient to obtain the best fit to the data. We integrate over the spatial and temporal profiles of the focal spot. That is, we numerically time integrate
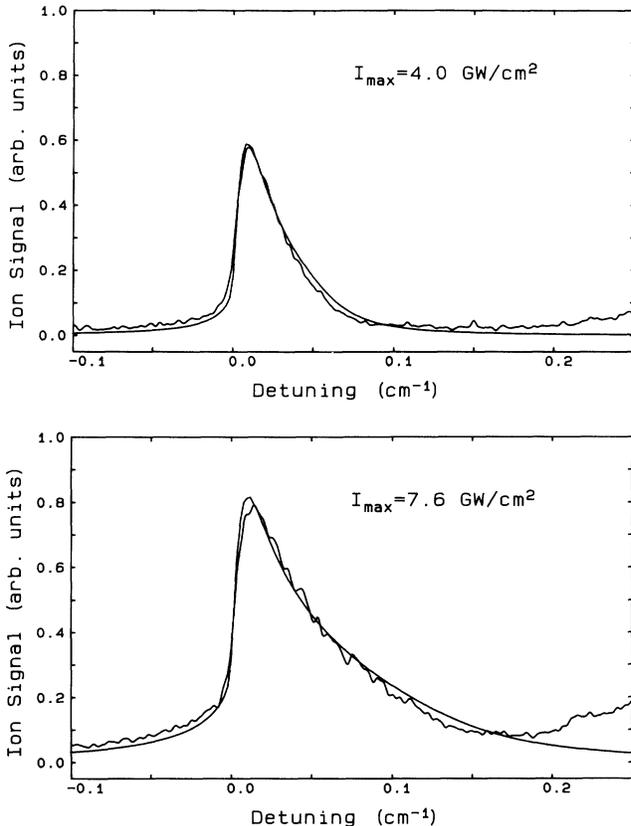
FIG. 4. Measured and calculated line shapes for two-photon resonant, three-photon ionization via the $2p^4\ ^3P_2 \rightarrow 3p\ ^3P_1$ resonance of atomic oxygen.

the optical Bloch equations over the actual temporal profile using two-photon effective coupling terms as described by Dixit, Levin, and McKoy [6] to prepare a data base covering a range of tunings and pulse fluences. This data base is used to perform the spatial integration for each laser tuning and pulse energy. We assume that the spatial intensity profile for the focal spot is Gaussian with the same peak intensity as the measured intensity profile. The true profile is the two-dimensional Fourier transform of the central Airy peak and thus has slightly more of its total energy in the center and less in the wings than a Gaussian spot, but we ignore this difference because the error introduced is 10% or less. Our best fit to the data indicates that the ac-Stark-shift coefficient is 5.1 ± 1.3 s^{-1}/W cm^{-2} or slightly less then the 6.7 s^{-1}/W cm^{-2} computed by Dixit, Levin, and McKoy [6]. Contributions to the experimental error from uncertainty in the focal diameter (20%), the pulse energy (5%), and the approximation to the time and spatial profile (10%), combine to produce the 25% uncertainty in the measured Stark coefficient.

IV. MEASUREMENT OF THE $3p\ ^3P$ TO $3s'\ ^3D^\circ$ "CORE CHANGING" TRANSITION STRENGTH

When two quantum levels are coupled by resonant light, their population oscillates between them at the

Rabi frequency [9]. In the absence of damping, if only the lower level is initially populated, the population of the upper level (P_{upper}) after the passage of a pulse of resonant light will be

$$P_{upper} = \frac{N}{2}(1 - \cos\theta) ,$$ (1)

where

$$\theta = \frac{\mu}{\hbar} \int \varepsilon(t)dt$$ (2)

and the driving electric field is defined by

$$E = \tfrac{1}{2}(\varepsilon e^{-i\omega t} + \varepsilon^* e^{+i\omega t}) .$$ (3)

The angle θ is the precession, or Rabi, angle and N is the number of atoms. The quantity μ is the strength of the transition, which in our case is the electric dipole transition moment. Thus if the time profile of the driving light pulse is well defined, we can calculate the Rabi angle as a function of pulse fluence assuming μ is known, or alternatively, μ can be derived from the observed dependence of the Rabi angle on pulse fluence as demonstrated by Haynam et al. [10]. This is the technique we use to measure the core-changing transition's strength. The appeal of this method is that only the easily measured temporal profile and fluence of the light pulse need to be calibrated to derive an absolute oscillator strength.

Figures 5 and 6 show how we first populate one of the fine-structure components of the $3p\ ^3P$ level using a pulse of 226-nm light focused to a spot a few hundred micrometers in diameter in the interaction region of the time-of-flight mass spectrometer. After a delay of about 50 ns to allow the O^+ pulse to decay in the particle detector, the second light pulse arrives and induces oscillation of the population between the $3p\ ^3P$ state and the $3s'\ ^3D^\circ$ state. This pulse produces very little additional ionization. As soon as this pulse is over, the third light pulse transfers the $3s'\ ^3D^\circ$ population to the $3p'\ ^3F$ state which autoionizes to furnish the observed ion signal.

The 800-nm light that induces the Rabi oscillation is produced by amplifying the light from a single-mode cw
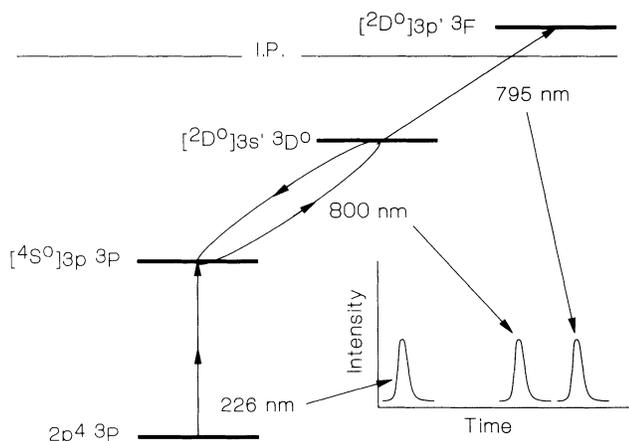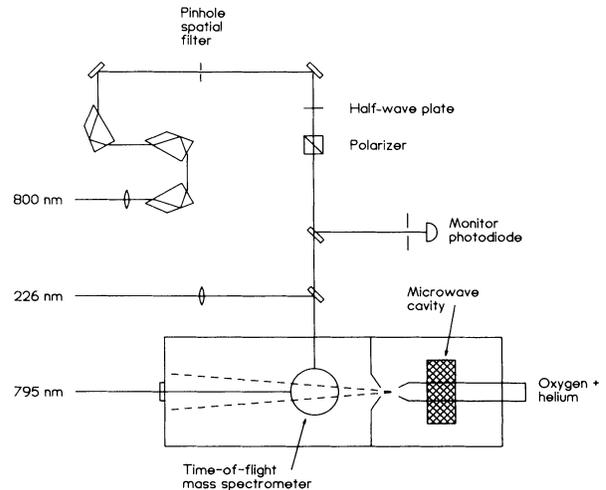
FIG. 6. Diagram of experimental layout for Rabi-oscillation measurements.

dye laser. It is spectrally and spatially filtered by passing it through three Pellin-Broca prisms and focusing it through a pinhole. This removes any amplified spontaneous emission originating in the dye amplifiers. After passing through the pinhole, the beam expands over a length of about 2 m so that at the interaction region it forms an Airy pattern with a central bright spot several mm in diameter centered on the much smaller 226-nm focal spot. This produces a uniform 800-nm light fluence for all the atoms that were prepared by the 226-nm pulse. The 800-nm fluence is varied by rotating a half-wave plate in front of a linear polarizer. We are careful to avoid clipping this beam on the edges of optical components to avoid fine-scale spatial modulation of the light in the interaction region.

The ionizing 795-nm light from the multimode pulsed dye laser crosses the first two lasers to efficiently ionize any atoms left in the $3s'\ ^3D^\circ$ state by the 800-nm measurement pulse. We typically collect between 10 and 1000 ions per pulse.

The fluence of the 800-nm-measurement pulse is measured using a photodiode located at a position optically equivalent to the interaction region but in a weak beam split off before the vacuum chamber. A 0.5-mm-diam aperture in front of the photodiode passes only the center portion of the Airy pattern. This photodiode is calibrated against a pyroelectric detector certified to 5% accuracy. The 800-nm beam is carefully centered on the 226-nm focal spot by temporarily inserting a second beam splitter in front of the vacuum chamber entrance window to direct the two beams to a second pinhole and photodiode pair at a point equivalent to the interaction spot. The 226-nm beam is centered on the pinhole and then the 800-nm beam position is adjusted to maximize its intensity on the pinhole. The linearly polarized 800-nm light enters the vacuum chamber through a Brewster window. Using this careful alignment procedure, the fluence at the interaction region can be measured to within 5%.

Rabi oscillations are simplest to analyze in a system where only one transition is being driven. In our case

FIG. 5. Diagram of our method of measuring Rabi oscillation in oxygen.

this means only one $|m_J|$ is involved. Because we can resolve the fine structure on each of the three steps, we achieve this for several cases by making use of the selection rules governing electric dipole transitions. Thus it is possible to measure individual fine-structure transition strengths for comparison with the ratios predicted by LS coupling and, if no significant deviation from LS coupling is observed, to obtain a value for the multiplet oscillator strength. We have measured Rabi oscillations for the following state sequences: $(J=2\rightarrow0\rightarrow1\rightarrow2, m_J=0)$, $(J=2\rightarrow1\rightarrow1\rightarrow2, m_J=\pm1)$, $(J=2\rightarrow1\rightarrow2\rightarrow3, m_J=\pm1)$, and $(J=1\rightarrow1\rightarrow1\rightarrow1, m_J=\pm1)$, where J refers to the sequence of J levels in the excitation pathway $2p^4\,^3P\rightarrow3p\,^3P\rightarrow3s'\,^3D°\rightarrow3p'\,^3F$ and m_J indicates the only magnetic sublevels ($\Delta m_J=0$) that contribute to the ion signal. Figure 7 shows a typical data set for the $J=1\rightarrow1\rightarrow1\rightarrow1$ case. Each data point represents the average of a few laser pulses. The solid curve is generated by numerically integrating the optical Bloch equations [11] including radiative decay of both the lower and upper level. The temporal profile of the light pulse is approximated by a Gaussian with the lower 5% clipped to account for the sharper turn on and turn off of the actual pulse compared with a Gaussian-shaped pulse. The height of the calculated curve is scaled to match the data and we vary the transition strength and detuning to find the best match.

We find that, within our measurement limits, LS coupling is valid and the multiplet $3p\,^3P$ to $3s'\,^3D°$ core-changing absorption oscillator strength is $2.4\times10^{-4}\pm10\%$. For comparison, there are two theoretic values for this oscillator strength available from the literature, 1.5×10^{-3} by Pradhan and Saraph [12] and 1×10^{-4} (velocity) to 2×10^{-4} (length) by Tayal and Henry [13]. Our experimental uncertainty is due to uncertainty in the calibration of pulse fluence (5%), our approximation to the actual temporal pulse shape in integrating the Bloch equations (5%), scatter in the data due to slight pulse-to-pulse variation in pulse shape (3%), and uncertainty in the detuning of the light from exact resonance (2%). Our reported value is also slightly sensitive to the value used for the radiative lifetimes of the $3p\,^3P$ and $3s'\,^3D°$ states. We have used lifetimes of 30 and 3.85 ns, respectively, based on reported measured [14] values.
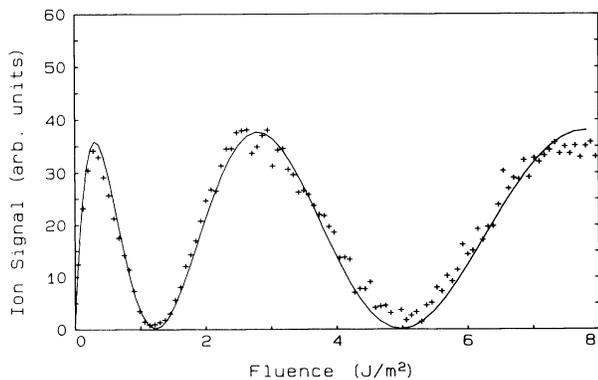
V. MEASUREMENT OF THE $3p'\,^{1,3}P$, ^3D AND ^3F AUTOIONIZING LIFETIMES AND $3s'\,^3D°$ TO $3p'\,^{1,3}P$, ^3D, AND ^3F TRANSITION STRENGTHS

If the lifetime of the autoionizing upper level of a resonantly driven transition is comparable to the duration of the light pulse, and if ions are collected during and after the pulse, the Rabi oscillations will appear damped. That is, the dips will not reach zero because some of the atoms decay during the pulse and thus contribute to the signal even for a 2π pulse. There will be residual modulation, however, because not all the atoms autoionize during the pulse and those that do not can be driven back to the nonionizing lower level. In this case the upper-state autoionization lifetime as well as the transition strength can be inferred from the shape of the curve of ion signal as a function of pulse fluence.

If the autoionizing lifetime is much less than the pulse duration, no atoms will be driven back to the lower level and the modulation will disappear. The Rabi oscillation will be replaced by a monotonic saturation curve. The pulse fluence at the knee of this saturation curve can then be used to find the absorption cross section of the transition. When the transition's linewidth is broader than the laser's a scan of the line gives the lifetime which, when combined with this cross section, yields the oscillator strength.

The reduction of modulation depth for short autoionizing lifetimes is the basis for our measurements of lifetimes and transition strengths involving the $3p'\,^{1,3}P$, ^3D, and ^3F levels. The technique and some results were presented in an earlier Letter [11]. A complete summary of results is given in Tables I and II. The oxygen atom is prepared in the $3s'\,^3D°$ state using two lasers, and the third laser subsequently drives the transition from this state to the autoionizing level of interest. The only substantial change from the core-change measurement discussed in Sec. IV is that here the grating-tuned dye laser is used as the second laser and an amplified single-mode dye laser is used to pump the final transition.

Figure 8 shows saturation curves for the $3s'\,^3D°$ to

FIG. 7. Rabi oscillations of the $3p\,^3P_1$ $m_J=1\rightarrow3s'\,^3D°_1$ $m_J=1$ transition. The crosses represent measurements and the solid curve is a computed fit based on integrating optical Bloch equations.

TABLE I. Autoionization rates for some even-parity levels of atomic oxygen.

Level	Autoionization rate (s^{-1})
$3p'\,^3D_1$	$1.5\times10^8\pm10\%$
$3p'\,^3D_2$	$4.5\times10^9\pm10\%$
$3p'\,^3D_3$	$3.7\times10^8\pm10\%$
$3p'\,^3F_2$	$3.2\times10^9\pm10\%$
$3p'\,^3F_3$	$3.1\times10^9\pm10\%$
$3p'\,^3F_4$	$1.9\times10^9\pm10\%$
$3p'\,^3P$	$1.5\times10^{14}\pm5\%$
$3p'\,^1P$	$7.2\times10^{10}\pm10\%$

$3p'\,^3D$ transitions. As before, each data point represents the average of a few laser pulses, while the solid curve is a fit to the data generated by numerically integrating the optical Bloch equations [11], again assuming a truncated Gaussian pulse shape. For the $3p'\,^3D$ $J=1$ and $J=3$ levels [Figs. 8(a) and 8(b)], the dipole transitions strength, lifetimes, and vertical scale are varied to fit the data. We find a multiplet absorption oscillator strength of $0.26\pm10\%$. Since the $3p'$ states radiatively decay predominantly to $3s'\,^3D^\circ$, this implies a radiative decay rate of 2.6×10^7 s^{-1} for the $3p'\,^3D$ states.

For the $J=2$ level [Fig. 8(c)], no modulation is evident so we scan the laser across the line to determine the
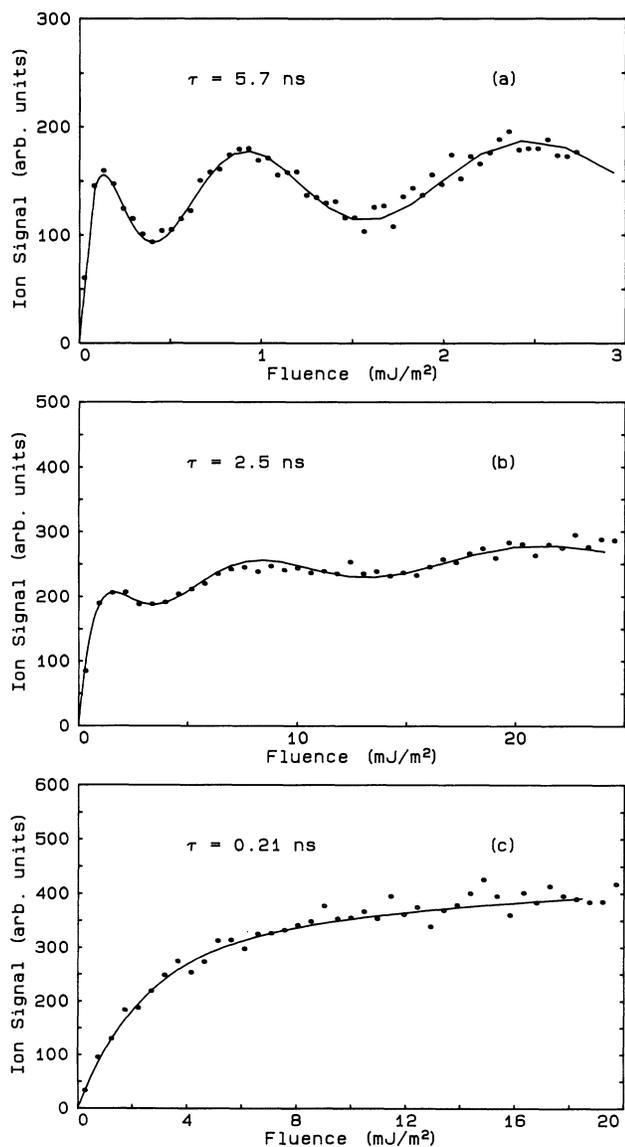
upper-state lifetime which is then used in integrating the optical Bloch equations. The lifetime is derived from the observed linewidth after subtracting the 10 MHz contributed by laser-frequency fluctuation and then deconvolving the laser linewidth and the residual Doppler width of 30 MHz. We then subtract the lower-level linewidth of 41 MHz corresponding to a 3.85-ns lifetime. We also iteratively correct for power broadening or saturation of the transition by using the uncorrected linewidth to calculate a transition strength and then use that to calculate a corrected linewidth and a corrected transition strength. This procedure converges in one iteration because saturation broadening is kept under 20%. Radiative decay $(2.6\times10^7$ s$^{-1})$ contributes only a fraction of a percent to the total width. Once the linewidth is known, only the dipole transition strength (and vertical scale) is varied while fitting the data of Fig. 8(c).

We used the following sequence of levels in these measurements of the $3p'\,^3D$ states:

$$(J=1\rightarrow1\rightarrow1\rightarrow1,m_J=\pm1)\,,$$

$$(J=2\rightarrow1\rightarrow2\rightarrow3,m_J=\pm1)\,,$$

$$(J=2\rightarrow1\rightarrow1\rightarrow1,m_J=\pm1)\,,$$

$$(J=2\rightarrow1\rightarrow1\rightarrow2,m_J=\pm1)\,,$$

$$(J=2\rightarrow1\rightarrow2\rightarrow1,m_J=\pm1)\,,$$

$$(J=1\rightarrow2\rightarrow3\rightarrow2,m_J=\pm1)\,,$$

and

$$(J=1\rightarrow2\rightarrow3\rightarrow3,m_J=\pm1)\,.$$

We find no significant deviation from LS coupling in the distribution of oscillator strength for this transition, and an l-to-l multiplet absorption oscillator strength of $0.26\pm10\%$ best fits our data. For comparison, Pradhan and Saraph [12] compute a value of $0.31\pm25\%$. The lifetimes for the three fine-structure levels are 5.6, 0.22, and 2.5 ns for $3p'\,^3DJ=1$, 2, and 3, respectively. The experimental uncertainties in these numbers are $\pm(10-15)\%$ as discussed in Sec. IV.

In contrast to the $3p'\,^3D$ states, the $3p'\,^3F$ $J=2$, 3, and 4 levels all have lifetimes short compared with the laser-pulse duration so we see no modulation in the saturation curves. As in the case of the $3p'\,^3D_2$ state above, we independently measure a linewidth and saturation curve to obtain the lifetime and oscillator strength. Figure 9 shows typical data, in this instance for the $3s'\,^3D_3^\circ$ to $3p'\,^3F_3$ transition. From the observed widths, we deduce lifetimes of 0.31, 0.32, and 0.53 $(\pm10\%)$ ns for the $J=2$, 3, and 4 levels, respectively. The radiative contribution to this width is negligible assuming a reasonable oscillator strength for $3p'\,^3D^\circ$ to $3p'\,^3F$. In fact, the multiplet absorption oscillator strength is found to be $0.48\pm20\%$. This is compared with values from previous work in Table II. For the $3p'\,^3F$ measurements, we used the transitions $(J=2\rightarrow2\rightarrow3\rightarrow4$, $m_J=0,\pm1,\pm2)$, $(J=1\rightarrow2\rightarrow3$ $\rightarrow3,m_J=\pm1)$, and $(J=2\rightarrow1\rightarrow1\rightarrow2,m_J=\pm1)$. The larger experimental uncertainty in oscillator strength here is due chiefly to greater uncertainty in fitting an un-

FIG. 8. Points represent measurements of ion signal and the solid curves are computed fits based on integrating optical Bloch equations. The lifetimes shown are those for the solid curves fitted to the data. The transitions are $3s'\,^3D^\circ\rightarrow3p'\,^3D$ (a) $J+1$, $m_J=\pm1$ to $J=1$, $m_J=\pm1$, (b) $J=2$, $m_J=\pm1$ to $J=3$, $m_J=\pm1$, and (c) $J=1$, $m_J=\pm1$ to $J=2$, $m_J=\pm1$.

TABLE II. Multiplet absorption oscillator strengths of atomic oxygen.

Transition	Measured oscillator strength (This work)	Measured oscillator strength (Previous work)	Theoretic oscillator strength
$3p\ ^3P \rightarrow 3s'\ ^3D°$	$2.4 \times 10^{-4} \pm 10\%$		1.5×10^{-3a} $(1-2) \times 10^{-4b}$
$3s'\ ^3D° \rightarrow 3p'\ ^3P$	$0.35 \pm 25\%$		0.26^c 0.20^g
$3s'\ ^3D°_1 \rightarrow 3p'\ ^1P_1$	$6.7 \times 10^{-5} \pm 20\%^c$		
$3s'\ ^3D° \rightarrow 3p'\ ^3D$	$0.26 \pm 10\%$	0.36^d	$0.31 \pm 25\%^a$ $0.33 \pm 10\%^f$ 0.32^g
$3s'\ ^3D° \rightarrow 3p'\ ^3F$	$0.48 \pm 20\%$	0.58^d	$0.5 \pm 25\%^f$

[a]Pradhan and Saraph [12].
[b]Tayal and Henry [13].
[c]J to J oscillator strength.
[d]Jürgens [21].

[e]Kelly [22].
[f]Wiese, Smith, and Glennon [23].
[g]Hofsaess [24].

modulated saturation curve compared with a modulated one.

We have located the $3p'\ ^3P$ level and find that it is much broader than the D or F levels. Because we cannot scan the single-mode laser over the full width of this level, we use it to drive the core-changing transition and adjust its fluence to the first Rabi peak. The grating-tuned

laser, operating on several longitudinal modes, is used to scan the autoionizing resonance. The pulse fluence of this laser is held constant at 4 mJ/cm^2 during the scan. Using Exciton laser dyes LDS751 and LDS698, we tuned over the range 670–760 nm which contains most of this autoionizing resonance. We used two sequences of J levels: $(J = 2 \rightarrow 2 \rightarrow 3 \rightarrow 2, m_J = 0, \pm 1, \pm 2)$ and $(J = 2 \rightarrow 0 \rightarrow 1 \rightarrow 0, m_J = 0)$. The fine structure is not resolved, but only one J level of the upper state can contribute in each case. We find the linewidth is the same for autoionizing states with $J = 2$ and 0, within our measurement limits. We again used a saturation curve of ionization versus pulse fluence at the center of the resonance to find the following peak absorption cross sections: 4.5×10^{-16} cm^2 for the $J = 1 \rightarrow J = 0$ transition and 3.7×10^{-16} cm^2 for the $J = 3 \rightarrow J = 2$ transition. After correction for power broadening, the width (FWHM) is 800 ± 40 cm^{-1} centered at $115\,165 \pm 30$ cm^{-1}. This implies a multiplet absorption oscillator strength from $3s'\ ^3D°$ of $0.35 \pm 25\%$ and an autoionization lifetime of 6.6 fs.

We also measured the width of the $3p'\ ^1P_1$ level and the oscillator strength for the transition $3s'\ ^3D°_1$ to $3p'\ ^1P_1$. Here the amplified cw light is used to pump the autoionizing level and the grating-tuned laser populates the $3s'\ ^3D°_1$ level. Because we found it difficult to tune the cw dye laser across the full width of this transition, we measured saturation curves at several fixed frequencies spaced evenly across the width. From the saturating intensity at each frequency we obtain an absorption cross section. The width of this autoionizing level is 0.38 ± 0.05 cm^{-1} (FWHM) and the $J = 1 \rightarrow J = 1$ absorption oscillator strength is $6.7 \times 10^{-5} \pm 20\%$. This width is nearly double the value of "about 0.20 cm^{-1}" quoted by Eriksson and Isberg [2].

In our analysis we have ignored direct photoionization to the $^4S°$ continuum from the $3s'\ ^3D°$ level because this cross section is much smaller than that for the autoionizing states. The line shapes show no evidence of asymmetry due to interference between these two pathways.

A sufficiently strong dc electric field in the ionization region will mix the state under study with nearby states
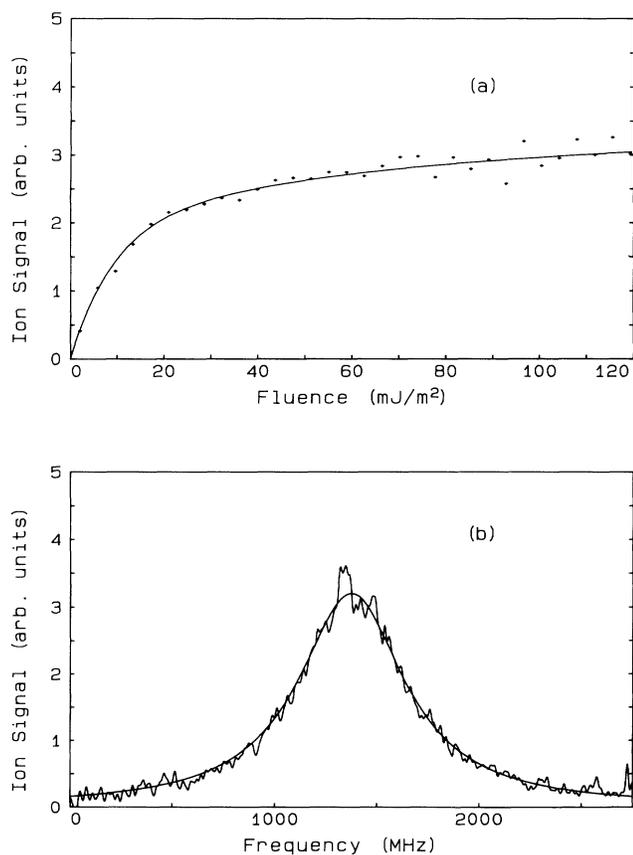
FIG. 9. (a) Saturation curve fit to data for the $3s'\ ^3D°_3 \rightarrow 3p'\ ^3F_3$ ($m_J \pm 1 \rightarrow m_J = \pm 1$) transition. (b) Lorentzian line-shape fit to measured line shape for the same transition.

of opposite parity. In particular, the $3s''\,^3P^\circ$ level is only about 600 cm^{-1} from the $3p'\,^3D$ level. This state autoionizes quite rapidly [3] so any electric-field-induced admixture could shorten our measured lifetimes. This sort of lifetime modification has been observed by Kelleher, Delpech, and Weiner [15] and Baier et al. [16]. To determine whether this is important in our measurements, we varied the dc electric field from 25 to 1000 V/cm and found no change in lifetime for the $3p'\,^3D_1$ state. Because there is no significant mixing in this case at 1 kV/cm, it is unlikely that the electric field affects any of the results reported here.

VI. LOCATION OF $4p'\,^3F$ STATES

With both the $3p\,^3P$ and $3s'\,^3D^\circ$ levels populated we scanned the third laser over the range of 800–383 nm searching for autoionizing levels. From the $3p\,^3P$ level this would cover odd-parity states from the lowest-energy ($^4S^\circ$) ionization limit to 114 730 cm^{-1}. We observe the $3s''\,^3P^\circ$ level, the only odd-parity autoionizing level in this range. From the $3s'\,^3D$ level, we would cover even-parity states up to 126 260 cm^{-1}. In addition to the states discussed above, we have found only the $4p'\,^3F$ manifold at 125 994, 126 001, and 126 009 cm^{-1} for $J=4$, 3, and 2, respectively (see Table III). The scanned laser in this case is a grating-tuned, pulsed dye laser with a linewidth of approximately 1 cm^{-1}. We did not attempt to scan these autoionizing resonances with higher resolution and cannot report line shapes. The wavelength of the laser was determined by the angle of its grating, a method that we find is accurate to approximately 2 cm^{-1}. We base our assignment of these levels on selection rules governing the strengths of the various lines of the multiplet. The $3p'\,^1F$ and ^1D states and the $4p'\,^3D$ states were not observable.

VII. DISCUSSION

It is interesting to consider the extreme variation of autoionizing lifetimes of the $3p'$ states which vary from about 6 ns to 6 fs. In the absence of spin-orbit interaction (pure LS coupling), the $3p'\,^3P$ state can autoionize to the $\epsilon p\,^3P$ contiuum state via Coulomb repulsion among the electrons. This fulfills the selection rules associated with this interaction [17], namely no change of parity, L, S, or J. Consequently, it should autoionize rapidly, and its 6.6-fs lifetime is comparable to other short-lived autoionizing states [18]. The $3p'\,^3F$ states likewise can autoionize to $\epsilon f\,^3F$ continuum states via the Coulomb interaction. In this case, however, the excited electron must switch from the $3p'$ to a ϵf orbit in addition to the core-state

TABLE III. New energy levels of atomic oxygen

State	Energy (cm^{-1})
$4p'\,^3F_2$	126 009±2
$4p'\,^3F_3$	126 001±2
$4p'\,^3F_4$	125 994±2
$3p'\,^3P$	115 165±30

change from ($^2D^\circ$) to ($^4S^\circ$). Because of the small interaction of an ϵf orbit with the core, this might be expected to yield a much smaller autoionization rate. In fact, it is smaller by about 4.5 orders of magnitude. However, the fact that the $J=4$ level lifetime is longer than the $J=2$ and 3 level lifetimes indicates that the electron spin must also play a role in the autoionization process. A spin-spin interaction [19] can mix $3p'\,^3P$ and $\epsilon p\,^5P$ levels into the $3p'\,^3F$. The former would affect only the $J=2$ and the latter only the $J=2$ and 3 states, whereas Coulomb mixing would affect all the J states equally. Dehmer, Luken, and Chupka [3] have shown that, for some of the odd-parity autoionizing states of oxygen, spin interactions do in fact produce lifetimes comparable to those we observe for the $3p'\,^3D$ and ^3F states.

In contrast to the $3p'\,^3P$ and ^3F states, the $3p'\,^3D$ states cannot autoionize via Coulomb repulsion because there is no odd-parity D state associated with the ($^4S^\circ$) core, whereas this interaction must preserve [19] parity, L, S, and J. Thus it must autoionize entirely through spin interactions. There are at least seven possible states that can mix with the ^3D states, but we will not discuss them all. However, for the $J=2$ state it appears that mixing with $3p'\,^3P_2$ must be dominant based on the observation that the $J=2$ state is both displaced to the red relative to its expected position about midway between the $J=1$ and 3 states, and broadened more than them. This would be expected if a state somewhat higher in energy with a short lifetime perturbed the $J=2$ state. Only the $3p'\,^3P_2$ state meets these criteria. Mixing with the $3p'\,^3P$ state also affects the $3p'\,^3D$ $J=1$ state, but not the $J=3$ state because the ^3P level has J values of 0, 1, and 2. Since the $^3D_3$ state autoionizes, some other states must also be involved.

In the LS-coupling approximation, the $3p'\,^1P_1$ state is also stable against autoionization because there is no singlet continuum associated with the ($^4S^\circ$) core. Although LS coupling is a good approximation at this low principal quantum number [20], the small amount of mixing of the very rapidly ionizing $3p'\,^3P_1$ state can produce an appreciable rate for the $^1P_1$ state. From a triplet state ($3s'\,^3D^\circ$), the peakcross sections for excitation of the singlet and triplet P_1 levels should be nearly the same if this explanation is correct since both the oscillator strength (proportional to the product of the width and height of the autoionizing resonance) and the width of the singlet resonance are proportional to the square of the mixing coefficient. In fact, the ratio of autoionizing rates is 4.8×10^{-4}, while the ratio of $J=1$ to $J=1$ oscillator strengths from $3s'\,^3D^\circ$ to $3p'\,^1P$ and ^3P is 1.1×10^{-3} or about twice the ratio of ionizing rates. The fact that the transition to the ^1P is about twice as strong as expected from this argument might indicate that the $3s'\,^3D^\circ_1$ state has a singlet component comparable to the triplet component of the $3p'\,^1P_1$ state.

Finally, we note that we could not observe autoionization of the $3p'\,^1D_2$ or $^1F_3$ levels nor of the $4p'\,^3D$ manifold when pumping from the $3s'\,^3D^\circ$ level. The fraction of $3p'\,^1D$ atoms that autoionize is unknown and may be small, accounting for our observation. However, the autoionization branching ratio for the $3p'\,^1F$ state is known

to be appreciable [20] so our observation indicates that the oscillator strength for the $3s'\,^3S°$ to $3p'\,^1F$ transition must be very small. We could observe the $4p'\,^3D$ (and $3p''^3D$) states by two-photon excitation from the $3p\,^3P$ level when one laser was very nearly resonant with the $3p\,^3P$ to $3s''\,^3P°$ transition. This indicates that the $3s'\,^3D°$ to $4p'\,^3P$ transition strength must be very small, con-

sistent with observations [4,5] of fluorescence from the $4p'\,^3D$ to $3s''\,^3P°$ transition, but not the $4p'\,^3D$ to $3s'\,^3D°$ transition. From our observations, the different J levels of $4p'\,^3D$ have quite different autoionizing rates similar to those of $3p'\,^3D$. For $4p'\,^3D$, the $J=1$ state ionizes very weakly, $J=2$ and 3 ionize more efficiently, with $J=2$ probably more efficient than $J=3$.

[1] K. B. S. Eriksson and H. B. S. Isberg, Ark. Fys. **24**, 549 (1963); K. B. S. Eriksson, *ibid.* **30**, 199 (1965); B. Isberg, *ibid.* **35**, 495 (1967); R. E. Huffman, J. C. Larrabee, and Y. Tanaka, J. Chem. Phys. **46**, 2213 (1967); M. Inguscio, P. Minutolo, A. Sasso, and G. M. Tino, Phys. Rev. A **37**, 4056 (1988); P. R. Brown, P. B. Davies, and S. A. Johnson, Chem. Phys. Lett. **133**, 239 (1987).

[2] A. A. Cafolla, T. Reddish, and J. Comer, J. Phys. B **22**, L273 (1989); R. E. Huffman, J. C. Larrabee, and Y. Tanaka, J. Chem. Phys. **46**, 2213 (1967); K. B. S. Eriksson and H. B. S. Isberg, Ark. Fys. **37**, 221 (1968); R. Frerichs, Phys. Rev. **34**, 1239 (1929); S. T. Pratt, P. M. Dehmer, and J. L. Dehmer, Phys. Rev. A **43**, 4702 (1991).

[3] P. M. Dehmer, W. L. Luken, and W. A. Chupka, J. Chem. Phys. **67**, 195 (1977); P. M. Dehmer and W. A. Chupka, *ibid.* **62**, 584 (1975); P. M. Dehmer, J. Berkowitz, and W. A. Chupka, *ibid.* **59**, 5777 (1973); R. A. Van Tassel, R. E. Huffman, and J. L. Roebber, *ibid.* **59**, 5926 (1973); W. H. Smith, J. Bromander, L. J. Curtis, H. G. Berry, and R. Buchta, Astrophys. J. **165**, 217 (1971). G. M. Lawrence, Phys. Rev. A **2**, 397 (1970). E. J. Knystautas, M. Brochu, and R. Drouin, Can. J. Spectrosc. **18**, 143 (1973). G. C. Angel and J. A. R. Samson, Phys. Rev. A **38**, 5578 (1988). J. P. Doering, E. E. Gulcicek, and S. O. Vaughan, J. Geophys. Res. **90**, 5279 (1985). E. C. Zipf and W. W. Kao, Chem. Phys. Lett. **125**, 394 (1986). J. D. Buck, S. Kröll, and W. K. Bischel (unpublished). P. van der Meulen, M. O. Krause, and C. A. de Lange, Phys. Rev. A **43**, 5995 (1991).

[4] R. Frerichs, Phys. Rev. **34**, 1239 (1929).

[5] K. B. S. Eriksson and H. B. S. Isberg, Ark. Fys. **37**, 221 (1968).

[6] S. N. Dixit, D. A. Levin, and B. V. McKoy, Phys. Rev. A **37**, 4220 (1988).

[7] K. Omidvar, Phys. Rev. A **22**, 1576 (1980); **30**, 2805 (1984); M. S. Pinzola, *ibid.* **17**, 1201 (1978); R. P. Saxon and J. Eichler, *ibid.* **34**, 199 (1986); E. J. McGuire, Sandia National Laboratory Report No. SAND85-2374, 1986 (unpublished).

[8] D. J. Bamford, L. E. Jusinski, and W. K. Bischel, Phys. Rev. A **34**, 185 (1986). D. J. Bamford, M. J. Dyer, and W. K. Bischel, Phys. Rev. A **36**, 3497 (1987).

[9] L. Allen and J. H. Eberly, *Optical Resonance and Two-Level-Atoms* (Wiley, New York, 1975). C. Cohen-Tannoudji, *Quantum Mechanics* (Wiley, New York, 1977).

[10] C.Haynam, B. Comaskey, M. Johnson, J. Paisner, and E. Worden, in *Proceedings of the Fourth International Symposium on Resonance Ionization Spectroscopy and Its Applications,* Institute of Physics Conference Series No.94, edited by T. B. Lucatorto and J. E. Parks (Institute of Physics, Bristol, UK, 1988), p. 41.

[11] A. V. Smith and T. D. Raymond, Opt. Lett. **16**, 33 (1991).

[12] A. K. Pradhan and H. E. Saraph, J. Phys. B **10**, 3365 (1977).

[13] S. S. Tayal and R. J. W. Henry, Phys. Rev. A **39**, 4531 (1989).

[14] W. H. Smith, J. Bromander, L. J. Curtis, H. G. Berry, and R. Buchta, Astrophys. J. **165**, 217 (1971). E. H. Pinnington, D. J. G. Irwin, A. E. Livingston, and J. A. Kernahan, Can. J. Phys. **52**, 1961 (1974); G. M. Lawrence, Phys. Rev. A **2**, 397 (1970); J. Bromander, N. Durić, P. Erman, and M. Larsson, Phys. Scr. **17**, 119 (1978); W. K. Bischel, B. E. Perry, and D. R. Crosley, Chem. Phys. Lett. **82**, 85 (1981); W. K. Bischel, B. E. Perry, and D. R. Crosley, Appl. Opt. **21**, 1419 (1982); J. P. Doering, E. E. Gulcicek, and S. O. Vaughan, J. Geophys. Res. **90**, 5279 (1985).

[15] D. E. Kelleher, J. F. Delpech, and J. Weiner, Phys. Rev. A **32**, 2230 (1985).

[16] S. Baier, M. Martins, B. R. Müller, and P. Zimmerman, Z. Phys. D **10**, 445 (1988).

[17] R. D. Cowan, *The Theory of Atomic Structure and Spectra* (University of California Press, Berkeley, 1981).

[18] J. Berkowitz, *Photoabsorption, Photoionization, and Photoelectron Spectroscopy* (Academic, New York, 1979).

[19] P. Feldman and R. Novick, Phys. Rev. **160**, 143 (1967).

[20] S. T. Pratt, P.M. Dehmer, and J. L. Dehmer, Phys. Rev. A **43**, 282 (1991); **43**, 4702 (1991).

[21] G. Jürgens, Z. Phys. **138**, 613 (1954).

[22] P. S. Kelly, J. Quant. Spectrosc. Radiat. Transfer **4**, 117 (1964).

[23] W. L. Wiese, M. W. Smith, and B. M. Glenon, *Atomic Transition Probabilities Vol. 1,* Natl. Bur. Stand. Ref. Data Ser., Natl. Bur. Stand. (U.S.) Circ. No. 4 (U.S. GPO, Washington, D.C., 1966).

[24] D. Hofsaess, J. Quant. Spectrosc. Radiat. Transfer **42**, 81 (1989).

Light beams

O beam

Quartz-boric acid
flow tube

Microwave
cavity

Cold trap and
diffusion pump

Time-of-flight
mass spectrometer

Cold trap and
diffusion pump

FIG. 3. Diagram of the atomic-beam and mass-spectrometer apparatus.